

THE FLAMINGOS EXTRAGALACTIC SURVEY

RICHARD J. ELSTON^{1,2}, ANTHONY H. GONZALEZ^{1,3}, ERIC MCKENZIE¹, MARK BRODWIN⁴, MICHAEL J. I. BROWN^{5,6},
 GUSTAVO CARDONA¹, ARJUN DEY⁵, MARK DICKINSON⁵, PETER R. EISENHARDT⁴, BUELL T. JANNUZI⁵, YEN-TING LIN⁷, JOSEPH
 J. MOHR^{7,8}, S. NICHOLAS RAINES¹, S. A. STANFORD^{9,10}, DANIEL STERN⁴

Draft version August 9, 2021

ABSTRACT

Using the Florida Multi-object Imaging Near-IR grism Observational Spectrometer (FLAMINGOS), we have conducted the FLAMINGOS Extragalactic Survey (FLAMEX), a deep imaging survey covering 7.1 deg² within the 18.6 deg² NOAO Deep Wide-Field Survey (NDWFS) regions. FLAMEX is the first deep, wide-area near-infrared survey to image in both the *J* and *K_s* filters, and is larger than any previous NIR surveys of comparable depth. The intent of FLAMEX is to facilitate the study of galaxy and galaxy cluster evolution at $1 < z < 2$ by providing rest-frame optical photometry for the massive galaxy population at this epoch. This effort is designed to yield a public data set that complements and augments the suite of existing surveys in the NDWFS fields. We present an overview of FLAMEX and initial results based upon $\sim 150,000$ *K_s*-selected sources in the Boötes field. We describe the observations and reductions, quantify the data quality, and verify that the number counts are consistent with results from previous surveys. Finally, we comment upon the utility of this sample for detailed study of the ERO population, and present one of the first spectroscopically confirmed $z > 1$ galaxy clusters detected using the joint FLAMEX, NDWFS, and *Spitzer* IRAC Shallow Survey data sets.

Subject headings: surveys — infrared: galaxies — galaxies: evolution — galaxies: clusters

1. INTRODUCTION

Two fundamental goals of extragalactic astronomy are to understand the star formation and mass assembly histories of the universe. It has become increasingly apparent in the last few years that the epoch $z = 1 - 2$ is critical for the evolution of both quantities. Current observations indicate that the bulk of stellar mass assembly in galaxies and $\sim 50\%$ of the total star formation occurs in this interval (Fontana et al. 2003; Dickinson et al. 2003; Rudnick et al. 2003). It is also during this epoch that we expect to witness the formation of the first massive galaxy clusters (for example, see Haiman et al. 2001). Observations at this epoch thus promise to provide a portrait of the universe during its most vibrant evolutionary period. Yet, in contrast to the wealth of data at low redshifts ($z < 1$, York et al. 2000; Colless et al. 2001; Kochanek et al. 2004) and high redshifts ($z = 2.5 - 4$, Steidel et al. 1998, 1999; Adelberger et al. 2003), this redshift regime remains less well explored due largely to the observational challenges historically associated with the “redshift desert” at $z = 1.4 - 2.5$ (for an overview, see Steidel et al. 2004). Recent spectroscopic work by a number of groups (e.g., Abraham et al. 2004; Coil et al. 2004; Steidel et al. 2004; Adelberger et al. 2005a,b; Mignoli et al. 2005) has begun to open this redshift window, but we currently lack large, homogenous samples comparable to those that exist at other redshifts. Moreover,

these existing programs are restricted to relatively small areas and are thus unable to probe the fraction of the massive galaxy population that resides in the overdense group and cluster environments. Infrared imaging surveys are a key first step towards generation of such samples. Infrared observations (both near-infrared and with IRAC on the *Spitzer Space Telescope*) have the advantage that the combined evolutionary and *k*-corrections are mild at this epoch, which means that uniform, roughly stellar mass-limited samples can be selected over a range of redshifts.

Using the Florida Multi-object Imaging Near-IR grism Observational Spectrometer (FLAMINGOS), we have conducted the FLAMINGOS Extragalactic Survey (FLAMEX). FLAMEX is a wide-area, near-infrared (NIR) imaging survey that is motivated by two basic considerations. First, FLAMEX is designed to probe the evolution and clustering of the massive galaxy population at $z = 1 - 2$ and to identify a sample of galaxy clusters at this epoch that can be used to study the assembly of cluster galaxies. The NDWFS fields are the targets of one of the most extensive panchromatic investigations in all astronomy, with space- and ground-based imaging and spectroscopic programs spanning radio to X-ray wavelengths (Jannuzzi & Dey 1999; Rhoads et al. 2000; de Vries et al. 2002; Hoopes et al. 2003; Lonsdale et al. 2003; Eisenhardt et al. 2004; Kochanek et al. 2004; Pierre et al. 2004; Houck et al. 2005; Murray et al. 2005). The northern (Boötes) field in fact is the only wide-area survey region presently mapped by *Chandra*, *GALEX*, and *Spitzer* (with IRAC and MIPS).

FLAMEX provides a combination of area and depth in both *J* and *K_s* that is unique among current NIR surveys (see Table 1 and Figure 1). Coupling the FLAMEX data with the optical (and when available IRAC) photometry enables derivation of robust photometric redshifts (Brodwin et al., in prep., and Brown et al., in prep.), providing an efficient means of isolating large samples of massive galaxies at $z = 1 - 2$. This combination of mass selection and photometric redshifts over a wide area constitutes a powerful tool not only for galaxy

¹ Department of Astronomy, University of Florida, Gainesville, FL 32611

² Deceased

³ NSF Astronomy and Astrophysics Postdoctoral Fellow, anthony@astro.ufl.edu

⁴ Jet Propulsion Laboratory, California Institute of Technology, 4800 Oak Grove Drive, Pasadena, CA 91109

⁵ National Optical Astronomy Observatory, Tucson, AZ, 85726-6732

⁶ Department of Astrophysical Sciences, Princeton University, Peyton Hall, Princeton, NJ 08544-1001

⁷ Department of Astronomy, University of Illinois, Urbana, IL 61801

⁸ Department of Physics, University of Illinois, Urbana, IL 61801

⁹ Physics Department, University of California, Davis, CA 95616

¹⁰ Institute of Geophysics and Planetary Physics, Lawrence Livermore National Laboratory, Livermore, CA 94551

TABLE 1. NIR SURVEYS

Survey	Filter	Area (deg ²)	Depth
Skrutskie et al. (1997, 2MASS)	<i>JHK_s</i>	All Sky	<i>K</i> = 14.5
Gardner et al. (1996)	<i>K</i>	9.84	<i>K</i> = 15.6
Jannuzi & Dey (1999, NDWFS Boötes)	<i>K</i>	9.3	<i>K</i> = 18.6
Huang et al. (1997)	<i>K'</i>	8.23	<i>K'</i> = 16
FLAMEX	<i>JK_s</i>	7.1	<i>K_s</i> ≈ 19.3
Chen et al. (2002, LCIRS)	<i>H</i>	1.1	<i>H</i> ≈ 21.5
Drory et al. (2001, MUNICS)	<i>JK'</i>	~1	<i>K'</i> = 19.5
Kümmel & Wagner (2001)	<i>K</i>	0.91	<i>K</i> = 17
		0.61	<i>K</i> = 17.5
Szokoly et al. (1998)	<i>K_s</i>	0.6	<i>K_s</i> = 16.5
Huang et al. (2001, CADIS)	<i>K'</i>	0.2	<i>K'</i> = 19.75
Daddi et al. (2000)	<i>K_s</i>	0.19	<i>K_s</i> = 18.8
		0.12	<i>K</i> = 19.2
Glazebrook et al. (1994)	<i>K</i>	0.15	<i>K</i> = 17.3
Cristóbal-Hornillos et al. (2003)	<i>K_s</i>	5 × 10 ⁻²	<i>K_s</i> = 21
Minezaki et al. (1998)	<i>K'</i>	5 × 10 ⁻²	<i>K'</i> = 19
		6 × 10 ⁻⁴	<i>K'</i> = 21
Martini (2001)	<i>JHK</i>	3.4 × 10 ⁻²	<i>K</i> = 18.5
Cimatti et al. (2002, K20)	<i>K_s</i>	1.4 × 10 ⁻²	<i>K</i> ≥ 20
McLeod et al. (1995)	<i>K</i>	5.6 × 10 ⁻³	<i>K</i> = 20
		5.6 × 10 ⁻⁴	<i>K</i> = 21.5
Totani et al. (2001)	<i>K'</i>	1.1 × 10 ⁻³	<i>K'</i> = 23.5
Djorgovski et al. (1995)	<i>K</i>	8.3 × 10 ⁻⁴	<i>K</i> = 24
Moustakas et al. (1997)	<i>K</i>	5.6 × 10 ⁻⁴	<i>K</i> ≈ 23.4 ^a
Bershady et al. (1998)	<i>JK</i>	4.2 × 10 ⁻⁴	<i>K</i> = 24

NOTE. — This table is intended to be a representative rather than comprehensive synopsis of previous surveys. The surveys are listed in order of decreasing survey area. We note that different authors quote different significance limiting magnitudes (for example 3 σ vs. 5 σ) within different size apertures, so the listed values provide only an approximate comparison of survey depths.

^aThis survey is split between two regions with limiting magnitudes of *K* = 23.1 and *K* = 23.7.

cluster detection and galaxy evolution studies, but also for selection of subsamples of rare objects that can be studied in greater detail.

Second, the addition of FLAMEX to the NDWFS repertoire provides the requisite deep NIR photometry that will be required by the next generation of NIR spectrographs. The astronomical community is poised to enter a new era in NIR spectroscopy, with multiobject instruments coming on line at multiple 8-10m class telescopes (MOIRCS at Subaru, FLAMINGOS II at Gemini South, EMIR at the Gran Telescopio Canarias). In this regard, the FLAMEX survey furthers one of the original aims of the NOAO Deep Wide-Field Survey by providing a wide-area public data set that can be used to select targets for spectroscopy.

In this paper we present an overview of the FLAMINGOS Extragalactic Survey. The science programs based upon the survey and details of the FLAMEX catalogs will be presented in other papers. The main aim in this manuscript is to provide relevant information regarding the general survey characteristics to the community in conjunction with the public data release, enabling researchers interested in the NDWFS fields to assess the applicability of this data set to their research programs. Towards this end, after presenting the data reductions and data quality we use the catalog in the Boötes field to provide two brief illustrations of the science topics that can be addressed with the FLAMEX data set.

The layout of this paper is as follows. We begin by describing the experimental design and observations in §2, including target sensitivities and field geometry. In §3 we present the

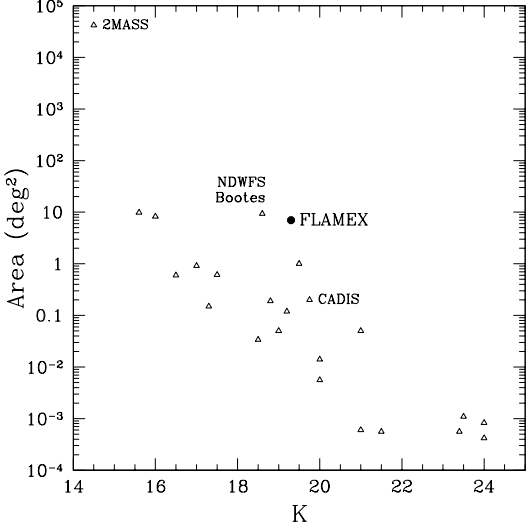


FIG. 1.— Comparison of FLAMEX with previous *K*-band surveys. The points show the published limiting magnitudes and areas for all the surveys listed in Table 1, except for the *H*-band LCIRS. Among the wide-area surveys shown, only FLAMEX, 2MASS, and MUNICS provide complete coverage in both *J* and *K_s* data. We note that no correction has been applied to correct for the different filters (*K*, *K'*, *K_s*) used by the different surveys, and that different authors quote different significance limiting magnitudes, so the data points provide only an approximate comparison of survey depths.

reduction procedure, followed by a description of the properties of the final Boötes catalog in §4. Illustrations of initial science and a discussion of the data release are given in §5, and the paper is summarized in §6. When relevant we assume a standard cosmology with $\Omega_M = 0.27$, $\Omega_\Lambda = 0.73$, and $H_0 = 70$ km s⁻¹ Mpc⁻¹.

2. EXPERIMENTAL DESIGN AND OBSERVATIONS

This survey is made possible by the FLorida Multi-object Imaging Near-Infrared Grism Observational Spectrometer (FLAMINGOS), which when commissioned was the world's first cryogenically cooled multi-object infrared spectrograph (Elston et al. 2003). FLAMINGOS has a fast all-refractive optical system that can be used at telescopes slower than f/7.5. This optical system, coupled with a 2048 × 2048 HgCdTe HAWAII-2 array, makes FLAMINGOS a very efficient wide-field imager when used on fast, small aperture telescopes. For the FLAMEX survey we rely purely on FLAMINGOS' imaging capabilities and the wide field afforded by the Kitt Peak National Observatory 2.1m. At this telescope FLAMINGOS has a 21' × 21' field-of-view with 0.61" pixels.

2.1. Location and Field Geometry

We initially targeted rectangular 5 deg² regions within each of the two NDWFS fields. The FLAMEX survey chose the NDWFS fields due to the deep optical imaging that was in progress in these fields when the survey was begun, with the *B_WRI* data being essential for enabling derivation of accurate photometric redshifts. The even split between the two fields was designed to permit follow-up observations during both observing semesters and from both hemispheres, while still yielding coverage for large, contiguous regions. Finally, the angular size of the survey is driven by the requirement that we probe a sufficiently large volume to detect massive clusters at $z > 1$. For a standard Λ CDM cosmology, one expects a

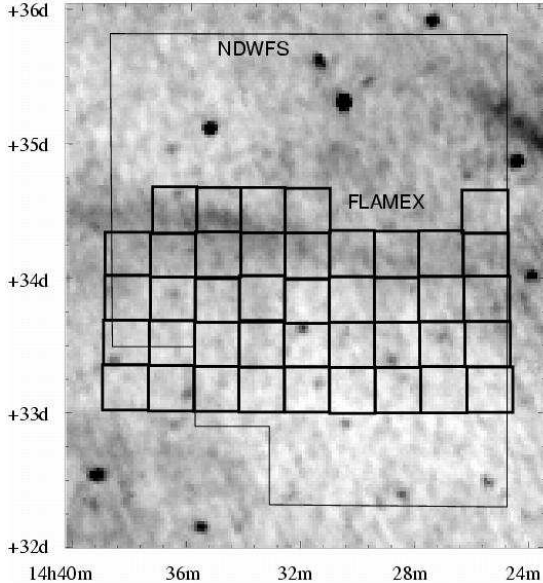


FIG. 2.— Final coverage for the FLAMEX survey in the NDWFS Boötes field, overlaid upon an IRAS 100 μ m image of the region (Wheelock et al. 1994). The boxes denote individual FLAMEX pointings, with the extent of the full NDWFS field also displayed. In the Boötes region we cover a 4.7 deg² strip.

surface density of approximately 0.7–4 deg² clusters with $M > 10^{14} M_{\odot}$ at $z > 1$, depending upon the value of σ_8 .¹¹ Consequently, the survey must cover roughly 5–10 deg² to ensure detection of a sample of massive clusters at this epoch.

While the survey plan called for a total of 10 deg², in practice worse than expected weather (see below) limited the total coverage to 7.1 deg². In the northern (Boötes) field the survey covers a 4.7 deg² region in both J and K_s ; in the southern field (Cetus) the corresponding coverage is 2.4 deg². The final geometry of each field is shown in Figures 2–3. In Cetus, this geometry was driven by following considerations. First, we started with observations in the eastern part of the NDWFS field to best complement the shallower K -band imaging from the NDWFS survey (Jannuzi & Dey 1999, Dey et al., in prep.), which predominantly lies in the western part of the Cetus NDWFS field. Second, we attempted to both maximize overlap with the *Spitzer* Wide-Area Infrared Extragalactic Survey (Lonsdale et al. 2003, SWIRE), which overlaps with the eastern part of the NDWFS, and cover the Gemini Deep Deep Survey's (Abraham et al. 2004, GDDS) field in Cetus. The former provides valuable additional information for photometric redshifts and constraining galaxy populations at $z \gtrsim 1$, while the latter provides calibration for photometric redshifts in the redshift desert ($z \approx 1.5$ –2). Observations were conducted as a gridded series of pointings, with adjacent field centers separated by 20'.

2.2. Survey Specifications

The original technical specifications for the program prescribed imaging of the survey region in both J and K_s for 2 hours to reach depths of $J = 22$ and $K_s = 20.5$ (5 σ , Vega) within 2" diameter apertures, assuming 1.5" FWHM seeing,

¹¹ These surface densities are calculated analytically, and are insensitive to whether one uses the prescription from Sheth & Tormen (1999) or Jenkins et al. (2001).

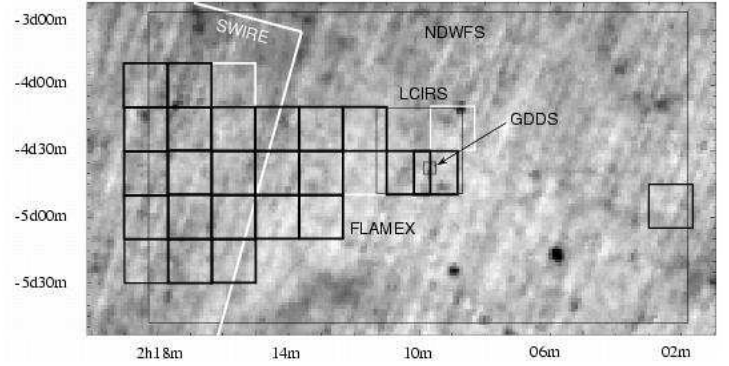


FIG. 3.— Final FLAMEX coverage in the NDWFS Cetus field. The image and boxes are the same as in Figure 2, except that three fields with incomplete J -band coverage are drawn in white. For Cetus we also overlay the locations of the SWIRE survey (large, white box), LCIRS (large, thin black box), and GDDS (small, thin black box). Near the GDDS field the overlap of the FLAMEX pointings was increased to increase the depth. The survey covers a total of 2.4 deg² in both J and K_s in Cetus, with an additional 0.3 deg² in K_s .

which for a point source is equivalent to total magnitudes $J = 21.4$ and $K_s = 19.9$. The final catalog is shallower (see §4.1) due to both the instrumental aberrations and worse than expected image quality. The effective depth of the data are of course also a strong function of the ambient temperature (i.e. the sky brightness). We therefore initially imaged each field for two hours per filter, and then reimaged the shallower fields in later runs to obtain relatively uniform data.

2.3. Observing Procedure

The standard observing sequence for the survey consisted of a randomly ordered 5 \times 5 dither pattern, with 1' offsets about the pointing center. This pattern was repeated until the required total exposure time was achieved. Individual exposures times were dependent upon the ambient temperature, ranging from 20–60s in K_s and 90–120s in J . The typical background sky level in K_s was 20,000–25,000 counts, with a maximum allowed level of \sim 30,000 counts. Detector nonlinearity can be corrected to better than 1% up to 45,000 counts; the maximum allowed level is designed to ensure that 2MASS stars with $K_s \geq 12.5$, which are used for photometric calibration, have peak fluxes below this level.

2.4. Observing Conditions

Data were obtained on the KPNO 2.1m during an allocation of 97 nights spanning 2001 December to 2004 December. While photometric conditions were not required, usable data were obtained on only \sim 50% of these nights due to a combination of suboptimal weather conditions and telescope mechanical failures. Observations were coordinated with the NOAO Survey Program "Toward a Complete Near-Infrared Spectroscopic and Imaging Survey of Giant Molecular Clouds" (PI: Lada). The two surveys shared nights to maximize observing efficiency since the target fields for the two groups lie at complementary right ascensions.

3. REDUCTIONS

Survey imaging was reduced using the LONGLEGS pipeline (Roman et al., in prep., and Gonzalez et al., in prep.), which employs standard infrared reduction procedures. Lin-

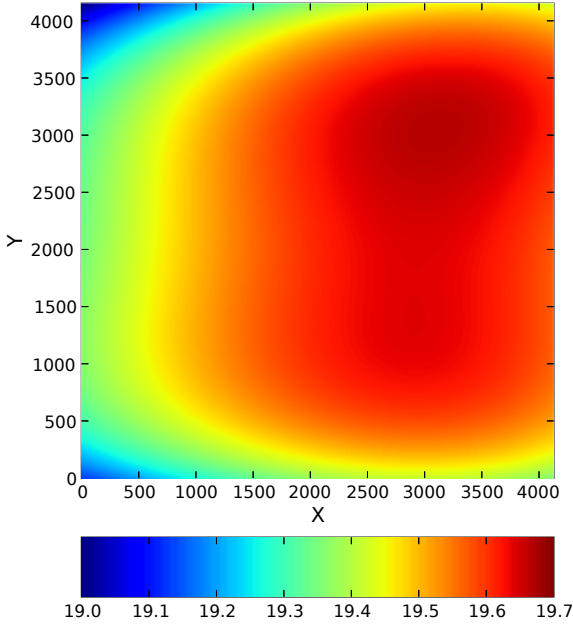


FIG. 4.— Map of the 50% completeness limit for $6''$ aperture magnitudes for K_s in one of the Boötes subfields. North is down and east is to the left. This map is generated using simulated elliptical galaxies with sizes consistent with the observed galaxy size distribution at $z = 1 - 2$ (Ferguson et al. 2004). As discussed in the text, the survey depth can vary by ~ 0.5 magnitudes within a given subfield.

earity correction,¹² dark subtraction, and flatfielding were all performed in the normal fashion. A running sky, typically comprised of 8 adjacent frames, was used for sky subtraction, with objects detected in the individual images masked before creation of the sky frames. The images were then transformed to correct for geometric distortion, doubling the number of pixels along both axes, and combined using a integer shift-and-add approach on these oversampled images. The resulting stacks are astrometrically and photometrically calibrated using the Two Micron All Sky Survey (2MASS) All Sky Data Release (Cutri et al. 2003). The final photometric calibration was computed using the average photometric offset for color-selected 2MASS stars in each field, weighted by the photometric errors. Field-to-field variations in the $J - K_s$ color of the full stellar locus are typically at the level of 0.02 magnitudes or less, indicating that the calibrations for the individual filters are good to this level or better.

Because the data for the survey were obtained over an extended time period, in many instances it was necessary to combine image stacks from different nights (or years). When combining, we weighted the images based upon the seeing, zeropoint, and rms noise in the input frames via the formula:

$$w = \frac{10^{0.4m_0}}{\sigma(FWHM)^2}, \quad (1)$$

where m_0 is the photometric zeropoint, FWHM is the full width half-maximum of the point spread function (PSF) at the field center, and σ is the rms noise in each image.

¹² Details related to the FLAMINGOS linearity correction and geometric distortions can be found at <http://flamingos.astro.ufl.edu>.

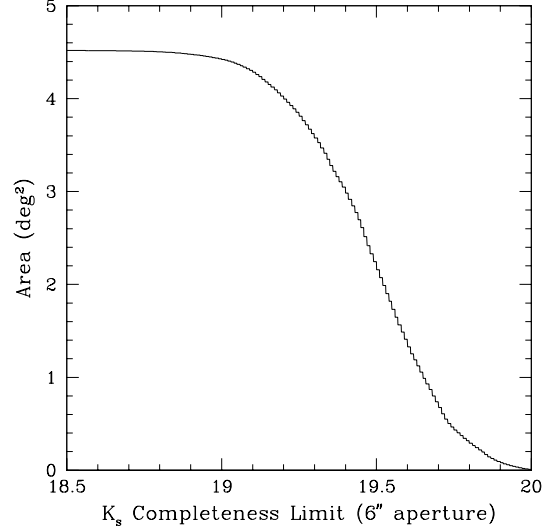


FIG. 5.— Survey area in Boötes as a function of the 50% completeness limit for the $6''$ diameter aperture. Over 90% of the survey region is complete to $K_s = 19.2$, with 50% being complete to $K_s = 19.5$. Note that while the total area covered in Boötes is 4.7 deg^2 , the effective area after accounting for masking and holes in the survey coverage is 4.55 deg^2 .

4. CATALOG PROPERTIES

We construct K_s -selected catalogs for each survey subfield using Source Extractor version 2.3 (SExtractor, Bertin & Arnouts 1996), using dual image mode to measure the J -band photometry within the same regions. Detection is performed in K_s with a $0.76''$ FWHM gaussian convolution kernel, and we impose a 5σ object detection threshold. Weight maps are also used to minimize detection of spurious. The catalogs for the individual subfields are then merged, with strict right ascension and declination boundaries defined between subfields to avoid double-counting of objects. We use completeness simulations, described below, to compute more realistic estimates of the magnitude errors than those provided by SExtractor, since the simulations can correctly account for correlated noise across pixels and the impact of background fluctuations. The typical magnitude errors from the simulations are roughly 2-3 times as large as the SExtractor errors for most apertures, and larger for the $20''$ aperture and the SExtractor automatic aperture (“AUTO”), which is designed to give an estimate of the total magnitude.

4.1. Survey Depth

The depth of the survey is position-dependent due to both instrumental aberration and shorter effective exposure times near the stack edges. The most appropriate way to quantify this variation is via completeness simulations for mock catalogs. We perform such simulations for each field to generate 50% completeness maps. Schematically, the design of the simulations is as follows.

First, we require a two-dimensional model for the point spread function for each field. For this we take an empirical approach – we use data from the dense stellar fields observed by the star formation survey (see §2.4) during the same observing run. We select the individual frames with the best seeing, and from these data generate a lookup table of the coordinates of bright, unsaturated stars. Several of the runs lack imaging from the star formation survey; for these we boot-

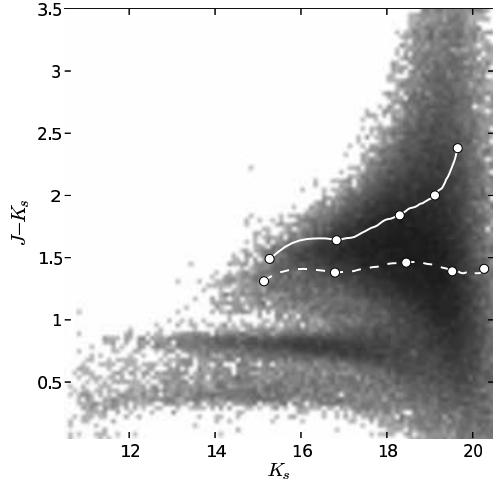


FIG. 6.— Infrared color-magnitude diagram for the Boötes field. The figure includes all objects with $K_s < 20.5$ that do not overlap with other objects ($\sim 84,000$). Objects are grouped in bins of width $\Delta K_s = 0.1$ mag and $\Delta J - K_s = 0.035$ mag. The greyscale runs from 0–100 objects per bin, with a logarithmic intensity scale. Note that the two horizontal sequences at $J - K_s = 0.4$ and $J - K_s = 0.8$ correspond to Galactic stars with types later than G5 and earlier than K5, respectively (Finlator et al. 2000). Intermediate type stars (K5 through G5) lie between these two sequences. The two curves are the predicted magnitudes and colors, based upon Bruzual & Charlot (2003) models with the Padova 1994 isochrones (Bertelli et al. 1994), for $M = 2 \times 10^{11} M_\odot$ galaxies with single burst (solid) and exponentially declining (dashed, $\tau = 10$ Gyr) star formation histories. The points correspond to $z = 0.25, 0.5, 1, 1.5, 2$.

strap off the survey data, using stars from the survey fields with the best seeing. To test the reliability of this bootstrap approach, we also run bootstrapped simulations for several fields with stellar template data. In these instances the completeness limits agree to $\lesssim 0.05$ mag in the field center and $\lesssim 0.1$ – 0.15 mag in the corners.

Second, we randomly select a location in the final image to insert a fake galaxy, and compute the corresponding location in each individual frame. We then generate a fake galaxy, convolve it with the nearest PSF star for each individual frame, combine these convolved model images, and add the galaxy into the final image.

For every field, in both the J and K_s filters, we insert 5000 fake galaxies with magnitudes spanning the completeness limit. The effective radii of these galaxies are chosen to uniformly span the range of values seen at $z = 1$ – 2 by Ferguson et al. (2004), who measured the distribution of half-light radii of distant galaxies in the Hubble Deep Field–North and Chandra Deep Field–South. Because the primary science goals of the survey focus upon the elliptical galaxy population at $z > 1$, we do not attempt to reproduce the full morphological distribution seen at this epoch. Instead, all mock galaxies used to calculate the completeness limits are pure bulges, with a distribution of effective radii in the range 0.07 – $0.5''$ (0.5–4 kpc at $z = 1$). While obviously a simplification, in practice the bulk of the objects detected in the survey are unresolved in the FLAMEX imaging data, making this a reasonable approximation even for disk galaxies. To verify this assertion, we reran the simulations in two subfields using only spiral galaxies with scale lengths $r_d = 0.6''$ (4.8 kpc at $z = 1$). The derived completeness limits were consistent to within 0.1 magnitudes with the results for pure bulges.

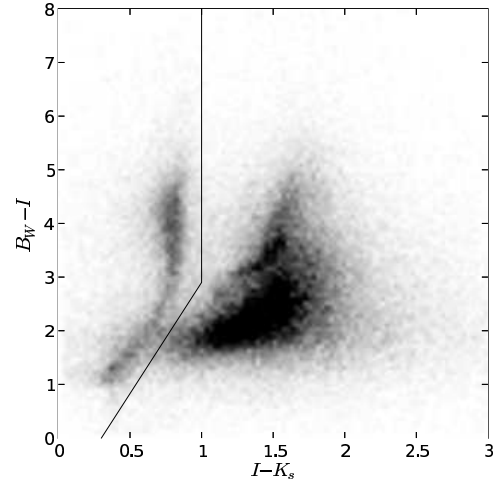


FIG. 7.— Color-color diagram for all FLAMEX sources, using $6''$ diameter aperture magnitudes. The solid line denotes the division between stars and galaxies that we utilize in §4.3.

We use the output of the simulations to derive two-dimensional maps of the 50% completeness limit for aperture and AUTO magnitudes measured with SExtractor. Figure 4 shows the derived map for a representative subfield. As expected, the off-axis aberrations degrade the survey depth in the corner regions. Statistical uncertainties for these maps can be derived via bootstrap resampling; in the image centers the completeness values have uncertainties of < 0.03 mag, while in the corners the uncertainties are ~ 0.1 mag. These values are slightly smaller than the systematic uncertainties evidenced by comparison of simulations using the bootstrap stellar templates with those from the star formation fields (see above).

In Figure 5, we plot the survey area as a function of the 50% completeness depth in the Boötes region for $6''$ diameter aperture magnitudes, incorporating the exposure maps to reproduce the effect of masking and dithering. More than 90% of the survey region is complete to $K_s = 19.2$, with 50% being complete to $K_s = 19.5$.

4.2. Star-Galaxy Separation in Color Space

FLAMEX is the first deep, wide-area near-infrared survey conducted in two filters. Our primary motivation for obtaining both J and K_s data was to efficiently isolate the $z > 1$ population, and these two bands, when combined with the optical NDWFS data (and/or with IRAC data), are particularly valuable for deriving robust photometric redshifts at $z \gtrsim 1$ (Brodwin et al., in prep.; Brown et al., in prep.). The combination of near-infrared (NIR) and optical photometry from FLAMEX and the NDWFS also find a number of other uses, including star-galaxy separation.

The variable PSF noted above precluded use of structural information to separate the star and galaxy populations in the FLAMEX data, but color information is an effective substitute. The $J - K_s$ color alone provides a simple means of performing star-galaxy separation, as can be seen in the color-magnitude diagram (Figure 6). Galactic stars with types earlier than K5 lie at $J - K_s = 0.8$; later types have bluer colors, with types later than M5 occupying a locus at $J - K_s = 0.4$ (Finlator et al. 2000). Galaxies, which occupy the redder lo-

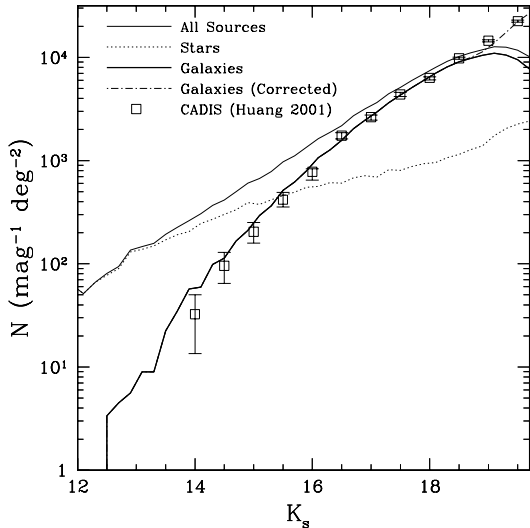


FIG. 8.— K_s differential number counts for the Boötes region. We use Source Extractor AUTO magnitudes, which for bright extended sources agree well with the 2MASS K20 total magnitudes. The thin solid line denotes the total number counts in the region, while the thick solid and dotted lines correspond to the color selected galaxies and stars, respectively. We also include the completeness-corrected galaxy number counts (dot-dashed line) and the galaxy number counts from the 20 arcmin² Calar Alto Deep Imaging Survey (CADIS; Huang et al. 2001), one of the largest previous K_s surveys to comparable depth. Our completeness-corrected number counts are consistent with the CADIS values over the full range, albeit with greater statistical precision (see also Figure 9).

cus of objects, are well-separated from the stars for $z \gtrsim 0.05$.

While the $J - K_s$ color alone provides a reasonable means of performing star-galaxy separation, inclusion of the NDWFS optical photometry can be used to improve the separation. We have generated a matched catalog combining the NDWFS third data release (DR3; Jannuzi et. al., in prep) and FLAMEX data. Detections in the different bands were matched if the centroids were within 1'' of each other. For extended objects, detections in the different bands were matched if the centroid in one band was within an ellipse defined using the second order moments of the light distribution of the object in another band.¹³ Figure 7 shows the $B_W - I$ vs $J - K_s$ color-color diagram for the survey using 6'' aperture magnitudes (sufficiently large that PSF mismatch between surveys is not an issue). The stellar sequence can be seen to cleanly separate from the galaxy locus, with the M stars being relatively redder in $B_W - I$ than the bluest galaxies, and the G stars remaining bluer in $J - K_s$. There remains a modest overlap between faint, nearby galaxies and the G star population, but the cut shown in Figure 7 overall provides an efficient means of separation with $\lesssim 5\%$ misidentification of galaxies at faint magnitudes (§4.3).

4.3. Number Counts

Galaxy number counts provide a useful means of testing the reliability of both the star-galaxy separation (§4.2) and the completeness simulations (§4.1). In Figure 8 we show the differential number counts for all sources in Boötes. Using the star-galaxy color separation, we split the number counts into the star and galaxy contributions. The slight upturn in the

stellar counts at $K_s \approx 19$ indicates that we may be misclassifying up to 5% of the galaxy population as stars if this is not an intrinsic feature of the stellar number counts. This systematic should be considered for any work involving either high-precision modelling of the number counts or statistical analysis of the local faint galaxy population.

Figure 8 also provides a comparison of the FLAMEX number counts with results from the 0.2 deg² Calar Alto Deep Imaging Survey (CADIS, Huang et al. 2001), one of the largest previous K_s surveys to comparable depth. Once a completeness correction is applied to the galaxy counts (dot-dashed curve), the faint-end FLAMEX number counts are consistent with CADIS to $K_s \gtrsim 19.5$. This agreement at the faint end provides validation for the completeness simulations described in §4.1.

Near-infrared galaxy number counts are also a classic diagnostic for constraining models of galaxy evolution (for example, Moustakas et al. 1997; Huang et al. 2001; Chen et al. 2002; Cristóbal-Hornillos et al. 2003). At these wavelengths the K-corrections are small, and the luminosities are both less affected by dust and less sensitive to recent star formation than optical number counts. These factors result in samples that are closer to mass-selected and hence simpler to model. While the magnitude regime probed by the FLAMEX data is not new, the large area afforded by this survey provides significantly greater statistical precision than previous work, enabling refined modelling. Realistic semianalytic models, which attempt to simultaneously match the observed counts in K_s and other passbands (such as Nagashima et al. 2002), are the optimal means for using this information. Such a detailed analysis is beyond the scope of this paper; however, in Figure 9 we compare with a simple classical model to illustrate both the utility of this data set and its precision relative to previous studies.

We use extendable galaxy number count model, *ncmod*, from Gardner (1998) with the same spectral templates and morphological mix of ellipticals and spirals as Gardner (1998). Similar to Cristóbal-Hornillos et al. (2003), we take the formation redshifts to be $z = 2$ for ellipticals and $z = 1$ for spirals, and add a component of star-forming dwarf galaxies with faint end slope $\alpha = -1.5$. For the general galaxy population we use the Schechter function parameters from Kochanek et al. (2001), while for the star-forming dwarf population we use the same prescription as Gardner (1998) and Cristóbal-Hornillos et al. (2003), but with $\phi_* = 3.5 \times 10^{-3} h_{50}^3$ Mpc⁻³ (roughly a factor of two lower than these studies). As found by Cristóbal-Hornillos et al. (2003), this type of model qualitatively fits the number counts over much of the observed magnitude range, albeit with some residual deviation. Most notably, FLAMEX and the other surveys yield fewer counts than the model at the brightest magnitudes. The FLAMEX number counts also exhibit an excess at the faint end ($K_s \gtrsim 19$) that is statistically significant with regard to the plotted Poisson uncertainties, albeit at a level that is small compared to the statistical uncertainties for most of the other samples shown. While an excess is also evident in the faintest CADIS data point, we caution against overinterpretation of this feature because this upturn occurs in the regime where our completeness correction is significant.

5. DISCUSSION

The fundamental motivation for the FLAMINGOS extragalactic survey is to facilitate systematic study of the evolution of massive galaxies and galaxy clusters at $z = 1 - 2$,

¹³ This ellipse was defined with the SExtractor parameters 2 × A_WORLD, 2 × B_WORLD, and THETA_WORLD.

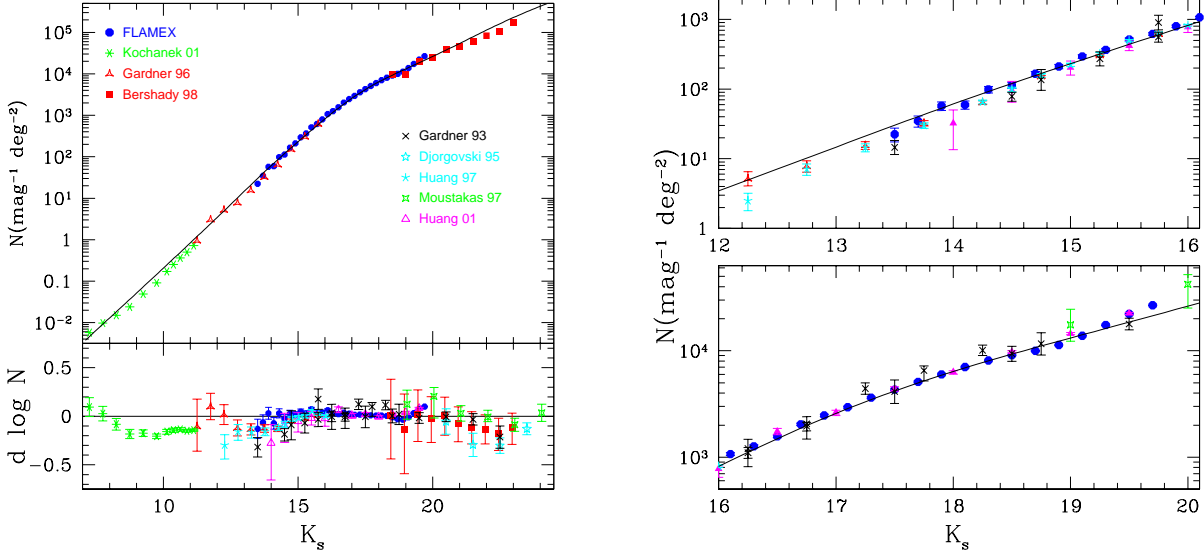


FIG. 9.— Differential number counts from FLAMEX and a representative sample of published data sets (Gardner et al. 1993; Djorgovski et al. 1995; Gardner et al. 1996; Huang et al. 1997; Moustakas et al. 1997; Bershady et al. 1998; Huang et al. 2001; Kochanek et al. 2001). The left panel shows the number counts for the full magnitude range probed by existing studies. The FLAMEX data and a subset of the data sets are shown in the upper part of the figure. Overlaid is a simple model constructed using *ncmod* that is similar to the one tested in Cristóbal-Hornillos et al. (2003). The formation epoch for ellipticals and spirals are set at $z = 2$ and $z = 1$, respectively, and a population of star-forming dwarfs (with a lower $\phi_* = 2.8 \times 10^{-3} h^3 \text{ Mpc}^{-3}$) is included to reproduce the faint end number counts seen in deep surveys. The lower part of the left panel shows the residuals relative to this model, including the error bars, for all data sets. For FLAMEX the error bars include only the Poisson uncertainty. There is good agreement between FLAMEX and previous studies in the magnitude range probed by FLAMEX. To facilitate a clearer comparison, the panels on the right show the same differential number counts, but restricted to the magnitude regime probed by FLAMEX. The different surveys are generally consistent to within the statistical uncertainties.

the epoch of peak global star formation and a critical era for both galaxy and galaxy cluster assembly. Complementing the existing programs in the NDWFS fields at other wavelengths, FLAMEX provides rest-frame optical photometry for the massive galaxy population at this epoch. The combination of the FLAMEX and NDWFS data enables the robust photometric redshifts and uniform selection criteria necessary for study of the galaxy and galaxy cluster populations at this epoch. In Boötes, the FLAMEX data also serves to bridge the gap between the existing optical and IRAC data sets, facilitating cross-association and investigation of optical drop-out populations.

The key scientific issues listed above will be the focus of a series of separate papers. In the following paragraphs, however, we supplement this overview of the survey with a few illustrations of basic applications of the FLAMEX data to provide the reader with a more quantitative sense of the science that can be achieved. In particular, we provide a brief analysis of the extremely red object (ERO) population and a synopsis of our galaxy cluster search before discussing our public data release. These items are intended simply to highlight a few uses of the FLAMEX data set – examples of other, multiwavelength programs (either underway or planned) that use FLAMEX include a high-redshift quasar search, investigation of the morphology-density relation at $z > 1$, construction of empirical optical to mid-IR galaxy spectral energy distributions, and investigation of the ensemble properties of distant galaxy clusters.

5.1. EROs

First discovered by Elston et al. (1988), extremely red objects (EROs) are traditionally defined as objects with $R - K_s > 5$ (although a range of definitions exist in the literature; see McCarthy 2004). While initially speculated to correspond

to a population of protogalaxies at $z > 6$, the ERO population is now understood to be predominantly comprised of two distinct types of galaxies – dusty starbursts and galaxies dominated by old stellar populations, both at $z \sim 0.8 - 2$ (e.g., Elston et al. 1989; Cimatti et al. 2002; Yan et al. 2004). For the dusty starbursts, strong extinction in the rest-frame near-ultraviolet drives the observed color; for the old galaxies, the red color is a simple consequence of the 4000 Å break passing redward of R -band. These two populations together are believed to constitute the dominant progenitor population for present-day elliptical galaxies, a belief that is supported by their space densities (Daddi et al. 2000) and strong spatial clustering (Daddi et al. 2000; Brown et al. 2005, but see Yan et al. 2004 for concerns with this interpretation). However, as a consequence of the strong spatial clustering and relatively low surface density of EROs, large area surveys are required for precise statistical analysis of the population.

The FLAMEX survey provides an order of magnitude increase in EROs sample size compared to other recent studies. We define EROs as being objects with $R - K_s > 5$ within a $6''$ aperture, imposing the additional requirement that $J - K_s > 1.2$ to eliminate potential contamination from stellar sources with spurious optical photometry (Figure 10a). By this definition, in the Boötes field alone we have over 7,000 EROs at $K_s < 19.5$ (Figure 10b); for comparison, the largest sample used thus far to study the clustering of EROs contained 671 objects down to $K = 18.4$ within a 1.4 deg^2 region in the NDWFS Boötes field (Brown et al. 2005). The FLAMEX counts are consistent with previous work, with the advantage that the large field enables identification of the brightest, rarest EROs and measurement of the number counts as bright at $K_s \approx 17$. This sample is also sufficiently large to begin to quantify the number density distribution as a joint function of magnitude

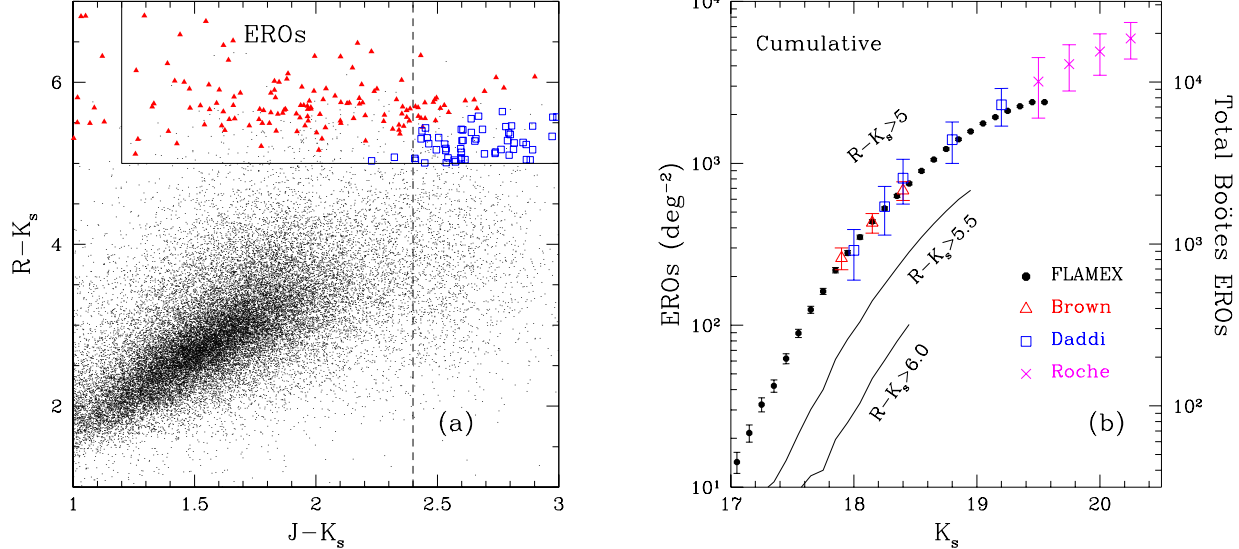


FIG. 10.—((a)) $R-K_s$ versus $J-K_s$ color distribution of FLAMEX sources in Boötes for a subset of sources with $17 < K_s < 19$. EROs are identified as objects with $J-K_s > 1.2$ and $R-K_s > 5$, with all colors calculated using 6'' aperture magnitudes. Filled triangles in this figure correspond to objects with $R > 24.5$ (roughly equivalent to an R -band SNR=4 in a 6'' aperture), and should be considered lower limits on the $R-K_s$ color. Roughly 40% of the EROS have lower limits in $R-K_s$. Open boxes correspond to objects that qualify as EROs from their $R-K_s$ color, but have only lower limits on the $J-K_s$ color. The vertical dashed line indicates that 50% of sources with $J-K_s > 2.4$ are undetected in the J -band magnitude. (b) Cumulative surface density of EROs detected within a 4.2 deg 2 subregion of the Boötes field. For $R-K_s > 5$ we present the FLAMEX Boötes data as filled circles and compare the observed number density with the results of several previous studies, including Daddi et al. (2001), Roche et al. (2002), and Brown et al. (2005). The FLAMEX counts for redder cuts ($R-K_s > 5.5$ and $R-K_s > 6$) are presented as solid lines down to limiting magnitudes corresponding to $R = 24.5$. We note that these curves are both roughly parallel to the $R-K_s > 5$ data. The total number of EROs in the Boötes field is shown on the right axis, demonstrating that the sample includes $> 7,000$ EROs with $K_s < 19.5$. We apply no completeness correction to the FLAMEX data, and hence the true surface density exceeds the FLAMEX points for $K_s \gtrsim 19$ (see Figure 8). There is also no correction applied to convert some of the other surveys from K to K_s , but for EROs the difference is minimal.

and color (see the curves for redder cuts in Figure 10b), providing a more stringent observational test for semianalytic evolutionary models.

5.2. Galaxy Clusters

One of the principal motivations for FLAMEX is identification of a large sample of galaxy clusters at $z > 1$. In the standard paradigm of hierarchical structure formation, we expect the formation of the first massive galaxy clusters to occur at $z = 1-2$. The comoving cluster number density at $M > 10^{14} M_\odot$ increases by roughly a factor of 30 between $z = 2$ and $z = 1$ (WMAP cosmology), with the precise number density and degree of evolution strongly sensitive to the details of the underlying cosmological model (particularly σ_8 and Ω_M). Aside from the cosmological applications (see for example Haiman et al. 2001; Borgani et al. 2001; Wang et al. 2004), detailed studies of homogeneous cluster samples at this epoch are essential for understanding the evolution of the cluster galaxy population and how the interplay between the galaxies and host clusters impacts this evolution. Observations at this epoch constrain the evolution of the halo occupation distribution (HOD), the formation epoch of cluster ellipticals, evolution of the color-magnitude relation, and the morphological evolution of cluster galaxies.

Infrared imaging, coupled with shorter wavelength photometry, provides an efficient means of detecting clusters at this epoch. The infrared data enable construction of roughly stellar mass-selected galaxy samples, and the combination of optical and infrared data enables derivation of photometric redshifts. The original plan for this program was to use the joint FLAMEX and NDWFS data sets to derive photometric redshifts, and then detect galaxy overdensities within redshift

slices. We developed a detection technique within this framework that is generically applicable to any photometric redshift catalog. The photometric redshift catalog is used to subdivide the data set into overlapping redshift bins, and we then employ a wavelet algorithm with bootstrap resampling to identify statistically significant overdensities on a fixed physical scale (a complete description will be provided in Gonzalez et al., in prep.).

Over the course of the survey this original plan has evolved in one significant regard. Joining forces with the IRAC Shallow Survey (Eisenhardt et al. 2004), we are now using the combination of NDWFS, FLAMEX, and IRAC (3.6 μ m and 4.5 μ m) photometry to derive more robust photometric redshifts (Brodwin et al., in prep.) and probe more deeply than would be possible with either the NDWFS and FLAMEX or NDWFS and IRAC data sets alone. The IRAC data are deeper than FLAMEX, allowing us to push further down the cluster luminosity function, while the FLAMEX data significantly reduce the scatter in photometric redshifts at $z \gtrsim 1.4$ (Brodwin et al., in prep.). We also now fold in the full redshift probability distribution for each source, which minimizes the noise from galaxies with poorly constrained redshifts. Additionally, our joint team is using the same technique in a complementary survey to detect clusters within the full 9.3 deg 2 NDWFS Boötes field using only the NDWFS and IRAC data (Eisenhardt et al., in prep.).

In this paper we present one of the first spectroscopically confirmed $z > 1$ clusters detected with the combined NDWFS, FLAMEX, and IRAC data sets, CL1432.5+3332.8 at $z = 1.11$ (Figure 11). To identify clusters within the FLAMEX region we perform a wavelet search using the photometric redshift probability distributions derived from the combined data sets,

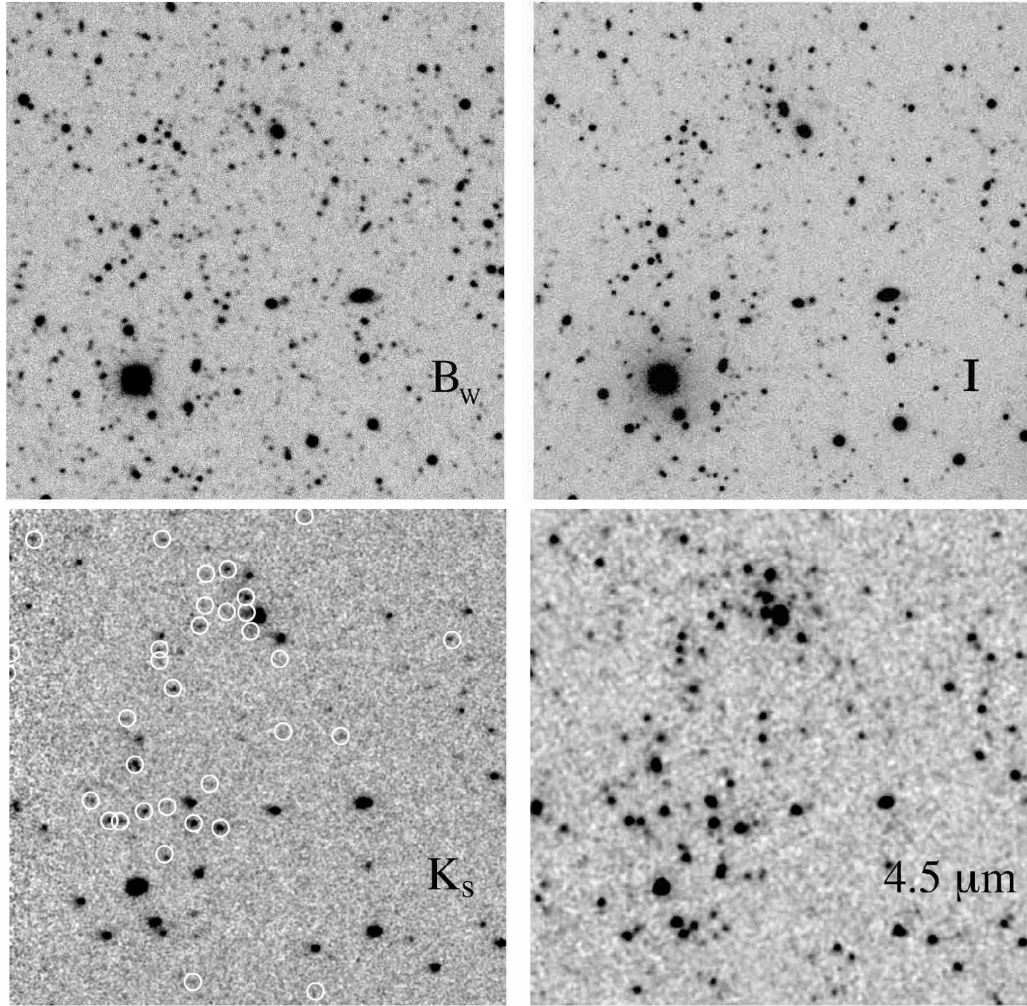


FIG. 11.— The four image panels, each $3' \times 3'$, show the core region of CL1432.5+3332.8 in B_W , I , K_s , and IRAC $4.5\mu m$. The cluster is visible as an excess of red galaxies in the K_s and $4.5\mu m$ bands, and in the K_s –band image we overlay circles to denote all galaxies with photometric redshifts $1 \leq z \leq 1.2$. The centroid of the cluster detection is located at $\alpha = 14h32m29.2s$, $\delta = +33d32m48s$ (J2000), which is near the dense clump of red galaxies in the upper, central part of the images.

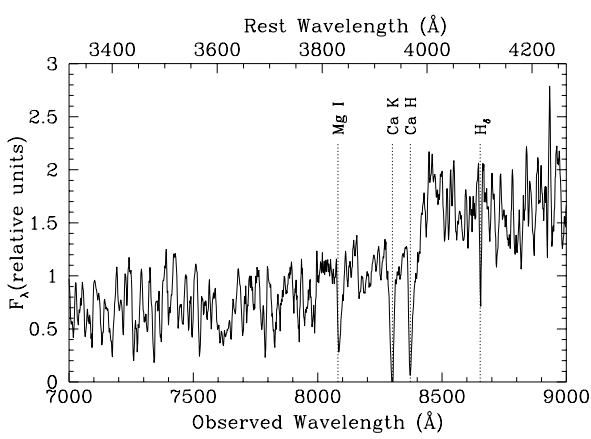


FIG. 12.— Spectrum of a galaxy at $z = 1.110$ in CL1432.5+3332.8, after smoothing with a 5 pixel boxcar filter. Several absorption features common to early-type galaxies are marked.

with the wavelet scale size defined to detect structures with physical scales $r \approx 200 - 800$ kpc. Monte Carlo simulations are then used to quantify the significance of each detection. This search identifies the cluster CL1432.5+3332.8 as one of the three highest significance overdensities at $z > 1$, with an estimated redshift $z = 1.2$ (Figure 11).

Spectroscopic confirmation of this candidate was obtained on 3 June 2005 UT using LRIS on Keck 1. We used a single slit mask for the observations which were carried out in clear conditions with 0.9 arcsec seeing. Five 1800s exposures were obtained, with the target galaxies shifted within the slitlets between each exposure. The data were reduced using standard long slit techniques (e.g. Stanford et al. 1997). The resulting redshifts include 8 galaxies at $1.10 < z < 1.12$. Of these, five exhibit absorption line features indicative of old stellar populations (Figure 12), arguing that we are observing a cluster with an established early-type population. A histogram of the redshifts is shown in Figure 13. The resulting velocity dispersion is $\sigma = 920 \pm 230$ $km s^{-1}$, as calculated using the gapper method (Beers, Flynn, & Gebhardt 1990), confirming that CL1432.5+3332.8 is a massive galaxy cluster.

The cluster CL1432.5+3332.8 is presented here as a proof

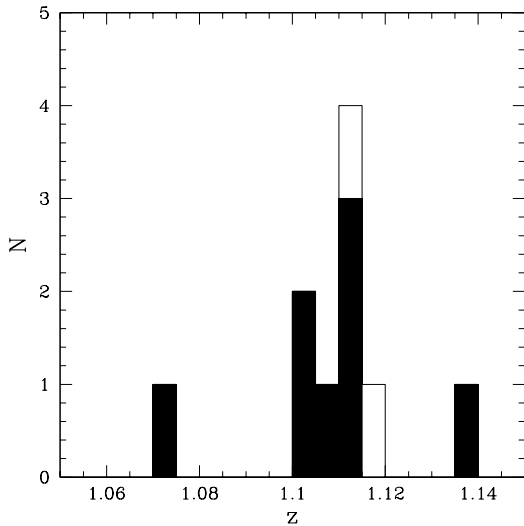


FIG. 13.— Redshift distribution from Keck observations of CL1432.5+3332.8. The solid histogram includes only galaxies with photometric redshifts $0.95 < z \leq 1.25$, while the open histogram includes all spectroscopic sources. The derived redshift and dispersion are $\langle z \rangle = 1.109$ and $\sigma = 920 \pm 230 \text{ km s}^{-1}$.

of concept to demonstrate that we can successfully identify clusters at $z > 1$ using the combined Boötes data sets. A single cluster detection of course cannot constrain the fidelity or completeness of catalogs derived with this data set. These are issues that will be addressed in subsequent papers, and in particular we refer the reader to Stanford et al. (2005), Brodwin et al. (in prep.) and Eisenhardt et al. (in prep.) for further explorations of the photometric redshifts and cluster catalogs derived from the NDWFS+FLAMEX+IRAC and NDWFS+IRAC data sets.

5.3. Public Catalogs

The FLAMINGOS Extragalactic Survey received time through the NOAO Large Survey Program and provides public access to the catalogs for the full FLAMEX region. The most recent version of the catalogs, accompanied by a detailed description, is posted on the web (starting September 30, 2005) at the following mirrors: <http://flamingos.astro.ufl.edu/extragalactic> and <http://www.noao.edu/noao/noaodeep/>.

6. SUMMARY

We present an overview of the FLAMINGOS Extragalactic Survey (FLAMEX), a near-infrared imaging survey conducted at the KPNO 2.1m with the FLAMINGOS instrument. FLAMEX is the first deep, wide-area NIR survey to image in both the J and K_s filters, and is larger than any previous surveys to comparable depth. Located within the NOAO Deep-Wide Field Survey regions, FLAMEX is designed to complement the NDWFS optical photometry and other existing multiwavelength public data sets, with the intent that it be a resource to the astronomical community. We therefore make the full catalogs from this program publicly available via the web pages listed in §5.3.

The survey area (7.1 deg^2) is divided between the northern (Boötes) and southern (Cetus) NDWFS regions, with 4.7 deg^2 in Boötes and 2.4 deg^2 in Cetus. We provide an initial characterization of the data set based upon the $\sim 150,000$ sources detected (5σ) within the Boötes field. The data in this region reach a median depth of $K_s \sim 19.3$ ($6''$ aperture), with a positionally dependent limiting magnitude that we model using extensive Monte Carlo simulations. Using the Boötes catalog in conjunction with optical NDWFS photometry we are able to perform a color-based star-galaxy separation that is robust for all sources except faint, blue galaxies at $z \sim 0$. We demonstrate that the Boötes number counts are fully consistent with results from previous, smaller area surveys down to $K_s = 19.6$, but with vastly reduced statistical uncertainty. We discuss the utility of this data set for quantifying the number density and clustering properties of the ERO population. The FLAMEX Boötes catalog alone contains an order of magnitude more EROs than any published studies. Finally, we describe one of the first spectroscopically confirmed clusters at $z > 1.1$, which was identified using photometric redshifts derived from the joint FLAMEX, NDWFS, and IRAC Shallow Survey catalogs.

The authors are deeply grateful to Elizabeth Lada for her many contributions to FLAMINGOS and our survey. In particular we thank her for critical assistance, advice, and guidance during the transfer of the survey leadership. Her personal and professional support were key to the success of the program. We also express our sincere thanks to the NOAO Survey TACs and NOAO for granting time for this survey through the NOAO Survey Program, and to Ron Probst and the observatory staff at Kitt Peak for support of the FLAMINGOS instrument. Additionally, we appreciate the efforts of the full FLAMINGOS instrument team at the University of Florida, including Jeff Julian, Kevin Hanna, and David Hon, and are grateful to Jonathan Gardner for his suggestions as referee. RJE acknowledges support from the National Science Foundation via a PECASE grant (AST-9875448). AHG acknowledges support from the NSF Astronomy and Astrophysics Postdoctoral Fellowship program under award AST-0407085 and from an NSF Small Grant for Exploratory Research under award AST-0436681. The work of MB, PRME, and DS was carried out at the Jet Propulsion Laboratory, California Institute of Technology, under a contract with NASA. JJM acknowledges support from the NASA Long Term Astrophysics award NAG 5-11415.

This publication makes use of data products from the Two Micron All Sky Survey, which is a joint project of the University of Massachusetts and the Infrared Processing and Analysis Center/California Institute of Technology, funded by the National Aeronautics and Space Administration and the National Science Foundation. This work is based in part on observations made with the *Spitzer Space Telescope*, which is operated by the Jet Propulsion Laboratory, California Institute of Technology, under a contract with NASA.

Facilities: KPNO 2.1m (FLAMINGOS), Keck 1 (LRIS), Spitzer (IRAC), KPNO 4m (MOSAIC-1)

REFERENCES

Adelberger, K. L., Steidel, C. C., Pettini, M., Shapley, A. E., Reddy, N. A., & Erb, D. K. 2005b, *ApJ*, 619, 697

Adelberger, K. L., Steidel, C. C., Shapley, A. E., & Pettini, M. 2003, *ApJ*, 584, 45

Bershady, M. A., Lowenthal, J. D., & Koo, D. C. 1998, *ApJ*, 505, 50

Bertelli, G., Bressan, A., Chiosi, C., Fagotto, F., & Nasi, E. 1994, *A&AS*, 106, 275

Bertin, E., & Arnouts, S. 1996, *A&AS*, 117, 393

Borgani, S. et al. 2001, *ApJ*, 561, 13

Brown, M. J. I., Jannuzzi, B. T., Dey, A., & Tiede, G. P. 2005, *ApJ*, 621, 41

Bruzual, G., & Charlot, S. 2003, *MNRAS*, 344, 1000

Chen, H. et al. 2002, *ApJ*, 570, 54

Cimatti, A. et al. 2002, *A&A*, 381, L68

Coil, A. L. et al. 2004, *ApJ*, 609, 525

Colless, M. et al. 2001, *MNRAS*, 328, 1039

Cristóbal-Hornillos, D., Balcells, M., Prieto, M., Guzmán, R., Gallego, J., Cardiel, N., Serrano, Á., & Pelló, R. 2003, *ApJ*, 595, 71

Cutri, R. M. et al. 2003, Explanatory Supplement to the 2MASS All Sky Data Release (Pasadena: IPAC), <http://www.ipac.caltech.edu/2mass/releases/allsky/doc/explsup.html>

Daddi, E., Broadhurst, T., Zamorani, G., Cimatti, A., Röttgering, H., & Renzini, A. 2001, *A&A*, 376, 825

Daddi, E., Cimatti, A., & Renzini, A. 2000, *A&A*, 362, L45

de Vries, W. H., Morganti, R., Röttgering, H. J. A., Vermeulen, R., van Breugel, W., Rengelink, R., & Jarvis, M. J. 2002, *AJ*, 123, 1784

Dickinson, M., Papovich, C., Ferguson, H. C., & Budavári, T. 2003, *ApJ*, 587, 25

Djorgovski, S. et al. 1995, *ApJ*, 438, L13

Drory, N., Feulner, G., Bender, R., Botzler, C. S., Hopp, U., Maraston, C., Mendes de Oliveira, C., & Snigula, J. 2001, *MNRAS*, 325, 550

Eisenhardt, P. R. et al. 2004, *ApJS*, 154, 48

Elston, R., Raines, S. N., Hanna, K. T., Hon, D. B., Julian, J., Horrobin, M., Harmer, C. F. W., & Epps, H. W. 2003, in Instrument Design and Performance for Optical/Infrared Ground-based Telescopes. Edited by Iye, Masanori; Moorwood, Alan F. M. Proceedings of the SPIE, Volume 4841, 1611–1624

Elston, R., Rieke, G. H., & Rieke, M. J. 1988, *ApJ*, 331, L77

Elston, R., Rieke, M. J., & Rieke, G. H. 1989, *ApJ*, 341, 80

Ferguson, H. C. et al. 2004, *ApJ*, 600, L107

Finlator, K. et al. 2000, *AJ*, 120, 2615

Fontana, A. et al. 2003, *ApJ*, 594, L9

Gardner, J. P. 1998, *PASP*, 110, 291

Gardner, J. P., Cowie, L. L., & Wainscoat, R. J. 1993, *ApJ*, 415, L9

Gardner, J. P., Sharples, R. M., Carrasco, B. E., & Frenk, C. S. 1996, *MNRAS*, 282, L1

Glazebrook, K., Peacock, J. A., Collins, C. A., & Miller, L. 1994, *MNRAS*, 266, 65

Haiman, Z., Mohr, J. J., & Holder, G. P. 2001, *ApJ*, 553, 545

Hoopes, C. G., Heckman, T. M., Jannuzzi, B. T., Dey, A., Brown, M. J. I., Ford, A., & GALEX Science Team. 2003, American Astronomical Society Meeting Abstracts, 203,

Houck, J. R. et al. 2005, *ApJ*, 622, L105

Huang, J.-S., Cowie, L. L., Gardner, J. P., Hu, E. M., Songaila, A., & Wainscoat, R. J. 1997, *ApJ*, 476, 12

Huang, J.-S. et al. 2001, *A&A*, 368, 787

Jannuzzi, B. T., & Dey, A. 1999, in ASP Conf. Ser. 191, Photometric Redshifts and the Detection of High Redshift Galaxies, ed. R. Weymann, L. Storrie-Lombardi, M. Sawicki, & R. Brunner (San Francisco: ASP), 111–117

Jenkins, A., Frenk, C. S., White, S. D. M., Colberg, J. M., Cole, S., Evrard, A. E., Couchman, H. M. P., & Yoshida, N. 2001, *MNRAS*, 321, 372

Kümmel, M. W., & Wagner, S. J. 2001, *A&A*, 370, 384

Kochanek, C. S., Eisenstein, D., Caldwell, N., Cool, R., Green, P., & AGES. 2004, American Astronomical Society Meeting Abstracts, 205,

Kochanek, C. S. et al. 2001, *ApJ*, 560, 566

Lonsdale, C. J. et al. 2003, *PASP*, 115, 897

Martini, P. 2001, *AJ*, 121, 598

McCarthy, P. J. 2004, *ARA&A*, 42, 477

McLeod, B. A., Bernstein, G. M., Rieke, M. J., Tollestrup, E. V., & Fazio, G. G. 1995, *ApJS*, 96, 117

Mignoli, M. et al. 2005, *A&A*, 437, 883

Minezaki, T., Kobayashi, Y., Yoshii, Y., & Peterson, B. A. 1998, *ApJ*, 494, 111

Moustakas, L. A., Davis, M., Graham, J. R., Silk, J., Peterson, B. A., & Yoshii, Y. 1997, *ApJ*, 475, 445

Murray, S. S. et al. 2005, *astro-ph/0504084*

Nagashima, M., Yoshii, Y., Totani, T., & Gouda, N. 2002, *ApJ*, 578, 675

Pierre, M. et al. 2004, *Journal of Cosmology and Astro-Particle Physics*, 9, 11

Rhoads, J. E., Malhotra, S., Dey, A., Stern, D., Spinrad, H., & Jannuzzi, B. T. 2000, *ApJ*, 545, L85

Roche, N. D., Almaini, O., Dunlop, J., Ivison, R. J., & Willott, C. J. 2002, *MNRAS*, 337, 1282

Rudnick, G. et al. 2003, *ApJ*, 599, 847

Sheth, R. K., & Tormen, G. 1999, *MNRAS*, 308, 119

Skrutskie, M. F. et al. 1997, in ASSL Vol. 210, The Impact of Large Scale Near-IR Sky Surveys, eds. F. Garzon et al. (Dordrecht: Kluwer Academic Publishing), 25–32

Stanford, S. A. et al. 2005, submitted to *ApJ Letters*

Stanford, S. A., Elston, R., Eisenhardt, P. R., Spinrad, H., Stern, D., & Dey, A. 1997, *AJ*, 114, 2232

Steidel, C. C., Adelberger, K. L., Dickinson, M., Giavalisco, M., Pettini, M., & Kellogg, M. 1998, *ApJ*, 492, 428

Steidel, C. C., Adelberger, K. L., Giavalisco, M., Dickinson, M., & Pettini, M. 1999, *ApJ*, 519, 1

Steidel, C. C., Shapley, A. E., Pettini, M., Adelberger, K. L., Erb, D. K., Reddy, N. A., & Hunt, M. P. 2004, *ApJ*, 604, 534

Szokoly, G. P., Subbarao, M. U., Connolly, A. J., & Mobasher, B. 1998, *ApJ*, 492, 452

Totani, T., Yoshii, Y., Maihara, T., Iwamuro, F., & Motohara, K. 2001, *ApJ*, 559, 592

Wang, S., Khouri, J., Haiman, Z., & May, M. 2004, *Phys. Rev. D*, 70, 123008

Wheelock, S. L. et al. 1994, NASA STI/Recon Technical Report N. 95, 22539

Yan, L., Thompson, D., & Soifer, B. T. 2004, *AJ*, 127, 1274

York, D. G. et al. 2000, *AJ*, 120, 1579